

Enhanced Photocatalytic Degradation of Methylene Blue Using TiO₂/ZnO/Fe₂O₃ Ternary Nanocomposites

Juliya A.P^{1,2}, Jayaram P^{3*}, Abdul Mujeeb V.M², Muraleedharan.K²

¹Department of Chemistry, University of Calicut Approved Research Centre, Malappuram, India

²Department of Chemistry, University of Calicut, Malappuram, India

³Department of Physics, Materials and Condensed Matter Physics Laboratory, Ponnani, India

Research Article

Received: 25-Nov-2022, Manuscript No. JOMS-22-81261; **Editor assigned:** 28-Nov-2022, Pre QC No. JOMS-22-81261 (PQ); **Reviewed:** 12-Dec-2022, QC No. JOMS-22-81261; **Revised:** 19-Dec-2022, Manuscript No. JOMS-22-81261(R); **Published:** 26-Dec-2022, DOI: 10.4172/2321-6212.11.1.001.

***For Correspondence:** Jayaram P, Department of Physics, Materials and Condensed Matter Physics Laboratory, Ponnani, India
E-mail: jayarampnair@gmail.com

Citation: Jayaram P, et al. Enhanced Photocatalytic Degradation of Methylene Blue Using TiO₂/ZnO/Fe₂O₃ Ternary Nanocomposites. RRJ Mater Sci. 2023;11:001.

Copyright: © 2023 Juliya AP, et al. This is an open-access article distributed under the terms of the Creative Commons Attribution License, which permits unrestricted use, distribution, and reproduction in any medium, provided the

Keywords: Methylene blue; Degradation; Photoluminescence; Nanocomposites; Transmission Electron Microscopy

ABSTRACT

Herein we report the synthesis and enhanced photocatalytic activity of ternary nanocomposite prepared *via* a single-step sol-gel process. Various characterization techniques were used for the analysis of the photocatalyst. XRD analysis clearly indicated the multiphase growth of nanocomposite. The average particle size obtained from Transmission Electron Microscopy (TEM) analysis of the photocatalysts TiO₂, TiO₂/ZnO, and TiO₂/ZnO/Fe₂O₃ were 19.1, 54.4, and 26 nm respectively. From BET analysis, it follows that there was a pronounced increase in the surface area of the ternary nanocomposite. The UV Visible DRS analysis indicated a considerable red shift of TiO₂/ZnO/Fe₂O₃ compared to that of TiO₂ and TiO₂/ZnO nanocomposite.

A comparative study on the photocatalytic performance of the prepared samples was performed using methylene blue as the model dye. The photocatalytic degradation of methylene blue in aqueous solutions was enhanced significantly when TiO₂/ZnO/Fe₂O₃ ternary nanocomposite was used as a photocatalyst. The consequences of the phase transition, surface features, and optical properties were compared and reported. The reduced photoluminescence intensity, decreased optical band gap energy and high surface area in ternary nanocomposite resulted in higher degradation of methylene blue under UV irradiation.

Keywords: Methylene blue; Degradation; Photoluminescence; Nanocomposites; Transmission Electron Microscopy

Keywords: Methylene blue; Degradation; Photoluminescence; Nanocomposites; Transmission Electron Microscopy

Keywords: Methylene blue; Degradation; Photoluminescence; Nanocomposites; Transmission Electron Microscopy

original author and source are credited.

INTRODUCTION

For the last few decades, we are under the threat of serious ecological imbalance that is being created by environmental pollution [1]. Toxic materials have accumulated in the environment to such a large extent that there needs a destructive mineralization process that roots out the pollutants from the ecosystem. Among the various toxic materials that have been discharged into nature, the dyes released from the textile industries occupy the forefront position [2]. Methylene blue is a heterocyclic aromatic compound which when released to the aquatic environment harms the aquatic organisms by depleting the content of oxygen and releasing toxic substances [3, 4]. Scientists have reported various methods for the remediation of methylene blue from the ecosystem [5-7].

The heterogeneous photocatalytic method is the competent method for the degradation of hazardous materials in the environment through the production of excitons upon illumination [8]. TiO₂ serves to be an efficient photocatalyst for the degradation of methylene blue [9]. Though there are many factors like cost effectiveness, nontoxic nature, resistance to corrosion, stability, etc. that attract TiO₂ as a good photocatalyst, the wide band gap and visible light inactivity render the scientist to modify the structural properties of TiO₂ [10-11]. Scientists use various approaches like doping with metals and non-metals, photosensitization, coupling with organic and inorganic material, etc. to increase the performance of TiO₂ as a photocatalyst [12, 13].

ZnO is a prominent photocatalyst with unique properties like nontoxicity, stability, low price, electro-optical, catalytic properties etc., [14, 15]. The attractive features of ZnO make it suitable for various applications like solar cells, diodes, antireflection coatings, sensors, etc., [16-18]. One way to improve the property of TiO₂ is to couple it with a suitable semiconducting metal oxide. Scientists have conducted various studies on the binary system TiO₂/ZnO. The studies prove that coupling enhances charge separation and modifies the electronic properties of the catalyst material [19-20]. For the past years efforts have been taken by researchers to develop the ternary photocatalytic system. The photocatalytic activity of the binary system can be improved by the introduction of a third system to the binary material. This further suppresses the electron-hole recombination and improves the photocatalytic efficiency of the system. Studies have reported that the doping of TiO₂ with Fe increases the visible light sensitivity of TiO₂ [21-23].

There are different preparative methods for the synthesis of metal oxides i.e., a dip coating method, ball milling process, electrochemical method, sol-gel method, etc. The sol-gel method is a low-cost method for the synthesis of nanomaterials with high purity and homogeneity [24-26]. In the present study, we report the synthesis and effectiveness of TiO₂, TiO₂/ZnO, and TiO₂/ZnO/Fe₂O₃ nanocomposite for the photocatalytic degradation of methylene blue. As there is a lack of studies on the photocatalytic degradation of methylene blue by TiO₂/ZnO/Fe₂O₃ we have focused our studies on this area. To elucidate the properties we report the structural, morphological, and optical properties of the compounds.

MATERIALS AND METHODS

High purity Tetrabutyl Titanate (TBOT), Zinc Nitrate (Zn (NO₃)₂·6H₂O) and Ferric Nitrate (Fe (NO₃)₃·9H₂O) and the analytic grade reagents ethanol and acetic acid were used for the sol-gel synthesis of the composite of TiO₂/ZnO/Fe₂O₃. 12.9 ml TBOT was initially dissolved in 51.1 ml absolute ethanol under vigorous stirring and 8.7 ml acetic acid, 0.66 ml water,

and 12.9 ml ethanol were added slowly until a yellow transparent solution was formed. Secondly, in a mixed solution of 20 ml absolute ethanol, 6.5 ml acetic acid, and 2.5 ml deionized water; $Zn(NO_3)_2 \cdot 6H_2O$ and $Fe(NO_3)_3 \cdot 9H_2O$ was added in the required amounts.

This second solution was mixed with the first solution drop wise with vigorous stirring at least for two hours. After aging this for 48 hours, the prepared sol was dried at $100^\circ C$ for 12 hours and then calcined at $500^\circ C$ for 5 hours in a microwave muffle furnace to obtain the end product. The same method was repeated for the synthesis of TiO_2 and TiO_2/ZnO in the absence of $Zn(NO_3)_2 \cdot 6H_2O$, $Fe(NO_3)_3 \cdot 9H_2O$, and $Fe(NO_3)_3 \cdot 9H_2O$ respectively. 50 ml of prepared standard methylene blue with a concentration of 10 M-4 M and 0.2 g of calcined photocatalyst (TiO_2 , TiO_2/ZnO , $TiO_2/ZnO/Fe_2O_3$) was added to the dye solution and stirred in the dark in UV reactor for 30 minutes in order to maintain the adsorption-desorption equilibrium.

This was followed by the performance of the reaction in the presence of UV light. The photocatalytic reaction was carried out in LZC-4X-Luzchem photo reactor provided with a bead. The reaction was monitored by withdrawing 3 ml aliquots at an interval of 20 minutes. After degradation, the solution was centrifuged to eliminate the effects of scattering before the evaluation of the photocatalytic activity.

The same experiment was conducted in direct sunlight with the most active catalyst. The intensity of sunlight at an interval of five minutes was measured using LUXMETER (LX-103). The diffraction patterns for X-ray diffraction analysis were recorded on Bruker AXS D8 advance diffractometer using $Cu-K\alpha$ radiation ($\lambda=1.5406\text{\AA}$).

The TEM analysis of the catalyst was performed on a JEOL/JEM 2100 transmission electron microscope. BET surface area was analyzed by BELSORP-max, an automatic gas adsorption measuring unit for gas adsorption, vapor adsorption, and chemisorption. To characterize the materials optically UV-Vis DRS measurement was done using a JASCO V-750 spectrophotometer and photoluminescence by JASCO Spectrofluorometer (FP-8300).

RESULTS AND DISCUSSION

XRD analysis

The nanocomposites formation was initially assessed by recording the XRD pattern indicated in Figure 1. The diffraction peaks 2θ at 25.39° , 37.85° , 48.11° , 62.76° , 69.05° , and 74.98° , respectively are the reflections of the (101), (004), (200), (204), (116), and (215) planes originated from the anatase phase of TiO_2 . While, 2θ at 27.5° , 36.14° , 41.3° , 44.16° , 54.37° , 56.69° , 64.12° , and 69.87° corresponds to the (110), (101), (111), (210), (211), (220), (310) and (312) plane of rutile phase of TiO_2 [27].

The mixed phase growth of TiO_2/ZnO was identified with the wurtzite hexagonal planes originating from points 31.8° , 34.5° , 36.2° , 47.6° , 6.8° , 62.9° and 68.1° along with the prominent TiO_2 phase [28]. Apart from TiO_2/ZnO planes, reflections at 23.99° , 30.3° , 32.87° , 35.42° , 40.53° , 49.05° , and 61.9° originated due to the hematite phase of Fe_2O_3 [29-31]. These peaks confirmed the formation of $TiO_2/ZnO/Fe_2O_3$ nanocomposites and the broad intense peaks are substantiating evidence of the growth of nano-sized grains.

This speculation is established with the grain size calculations performed by Scherrer equation and are displayed in Table 1. By means of Williamson and Smallman's formula, we were able to calculate the Dislocation density and presented it in table 1.

Figure 1. X-Ray Diffraction pattern of the compounds indicating composite formation as the number of cations increases.

Note: ■ $\text{TiO}_2/\text{ZnO}/\text{Fe}_2\text{O}_3$, ■ TiO_2/ZnO , ■ TiO_2 .

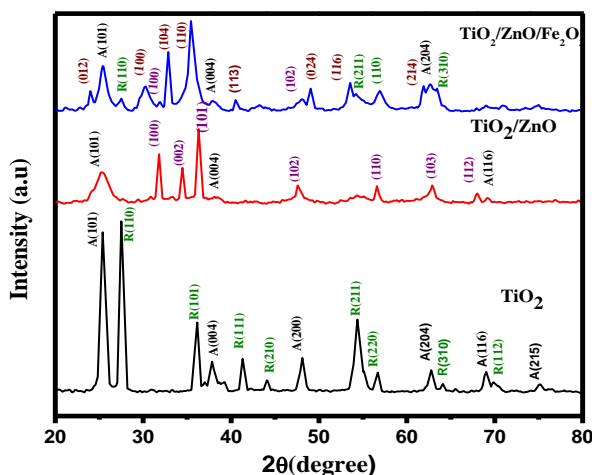


Table 1. Average grain size calculated from the Scherrer equation and dislocation density from Williamson-Smallman’s formula as well as the BET results, regression coefficient, and rate constant of TiO_2 , TiO_2/ZnO , and $\text{TiO}_2/\text{ZnO}/\text{Fe}_2\text{O}_3$.

Compound	Average Grain Size (nm)	Dislocation Density $\delta \times 10^{16} \text{m}^{-2}$	BET surface area (m^2/g)	Pore volume (cm^3/g)	Regression coefficient (R^2)	$K_{app}(\text{min})^{-1}$
TiO_2	22.53	0.2	29.1	0.029	0.99	0.007
TiO_2/ZnO	22.8	0.19	43.7	0.049	0.99	0.01
$\text{TiO}_2/\text{ZnO}/\text{Fe}_2\text{O}_3$	24.26	0.17	78.5	0.1335	0.93	0.02

Surface morphology: Transmission Electron Microscopy and Brunauer-Emmett-Teller analysis. The surface topography of TiO_2 , TiO_2/ZnO , and $\text{TiO}_2/\text{ZnO}/\text{Fe}_2\text{O}_3$ are displayed in Figures 2a-2j, comprising TEM, HRTEM images, and SAED ring patterns. The images divulge aggregated growth of particles in semi-globular shapes. In binary and ternary composites, the shapes of particles were unaltered roughly spherical in shape.

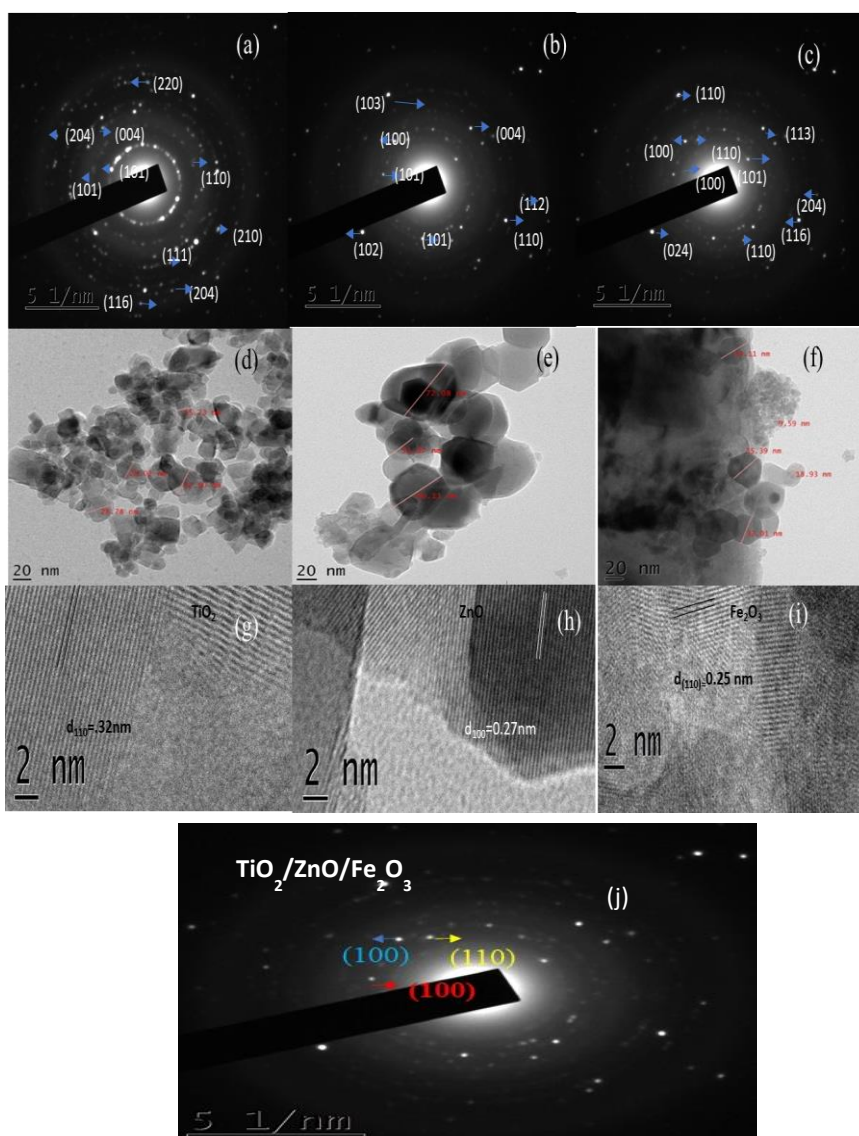
However, the average particle size obtained for TiO_2 , TiO_2/ZnO , and $\text{TiO}_2/\text{ZnO}/\text{Fe}_2\text{O}_3$ was 19.1, 54.4, and 26 nm respectively. From the high-resolution TEM image the gap between two fringes in TiO_2 , TiO_2/ZnO , and $\text{TiO}_2/\text{ZnO}/\text{Fe}_2\text{O}_3$ were 0.32, 0.27 nm, and 0.25 nm, which can be indexed to (110), (100) and (111) planes corresponding to TiO_2 , ZnO and Fe_2O_3 respectively (Figures 2g-2i).

The measurements obtained from the SAED rings for the three samples were consistent with the results of the XRD pattern. From the TEM image, it is evident that interfacial contact exists in the ternary nanocomposite. The BET results of the catalysts are shown in Table 1. As the results presented, the BET surface area of TiO_2 , TiO_2/ZnO , and $\text{TiO}_2/\text{ZnO}/\text{Fe}_2\text{O}_3$ were 29.1, 43.7, and 78.5 m^2/g respectively. Specific surface areas have a pronounced effect on photocatalytic activity.

The BET results revealed the presence of Zn^{2+} and Fe^{3+} ions significantly increased the surface area of the samples. The increase in the surface area of the ternary system can be attributed to the replacement of the Ti^{4+} (0.605 Å) which is

having lower ionic radii by Zn^{+2} (0.74 Å) and Fe^{3+} ions (0.645Å) that created imperfection in the crystal making the sample rough and disordered. This is expected to activate more sites on the surface of the catalyst and thus improved the photocatalytic activity [32].

Figure 2. (a) SAED patterns of TiO_2 , (b) SAED patterns of TiO_2/ZnO (c) SAED patterns of $TiO_2/ZnO/Fe_2O_3$ (d) TEM images of TiO_2 (e) TEM images of TiO_2/ZnO (f) TEM images of $TiO_2/ZnO/Fe_2O_3$ (g) HRTEM images of TiO_2 (h) HRTEM images of TiO_2/ZnO (i) HRTEM images of $TiO_2/ZnO/Fe_2O_3$ (j) SAED patterns of TiO_2 , TiO_2/ZnO and $TiO_2/ZnO/Fe_2O_3$.



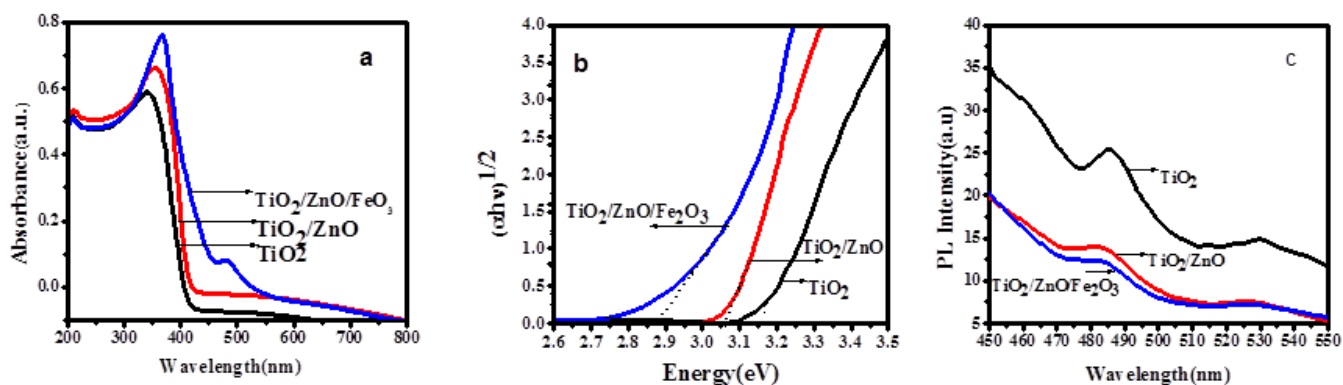
UV-visible DRS analysis and photoluminescence studies

The UV-visible DRS of TiO_2 , TiO_2/ZnO , and $TiO_2/ZnO/Fe_2O_3$ nanosystems was represented in Figures 3a-3c. The UV-visible spectra of TiO_2/ZnO were slightly red-shifted in comparison to the spectra of bare TiO_2 . This was further red-shifted in the ternary nanocomposite. The red shift of the ternary nanocomposite can be attributed to the promotion of electrons from the valence band of Fe_2O_3 to that of TiO_2 [33]. The optical band gap energies were estimated from the Kubelka-Munk plot and the corresponding values were 3.17 eV, 3.07 eV, and 2.9 eV for TiO_2 , TiO_2/ZnO , and

TiO₂/ZnO/Fe₂O₃ respectively. The reduction of the band gap may be explained by relating the structural deformation of the compounds, as the novel composite structure was formed as depicted by XRD. However, the incorporation of iron enhanced the visible light absorption power of the catalyst. The narrowing of the band gap of TiO₂/ZnO/Fe₂O₃ was expected to bolster the photocatalytic activity.

Figure 3c the PL spectrum of TiO₂, TiO₂/ZnO and TiO₂/ZnO/Fe₂O₃ are displayed. PL emission intensity is directly related to the electron-hole recombination; the higher the PL intensity photocatalytic rate will be lower. The materials exhibited two broad PL emission signals at 485 nm and 525 nm, the signal at 485 nm was due to the surface oxygen vacancies and the emission at 525 nm was due to the localized F⁺ centres on the surfaces of compounds [34, 35]. The surface oxygen vacancies will act as charge-trapping centres and prevent electron-hole recombination. The emission intensity of the PL spectra was obtained in the following order TiO₂>TiO₂/ZnO>TiO₂/ZnO/Fe₂O₃. The decrease in PL intensity indicated the lower recombination rate of photogenerated electron-hole pairs. The presence of ZnO and Fe₂O₃ in the crystal symmetry of TiO₂ has obviously resulted in the lowering of PL intensity. The results propound the photocatalytic activity can be higher in TiO₂/ZnO/Fe₂O₃ as it can suppress the combination between the photogenerated electrons and holes.

Figure 3. (a) UV-visible spectra of the samples recorded in diffuse reflectance mode (b) The optical band gap energy determined by using Kubelka-Munk theory (c) The photoluminescence spectra of the samples. Note: ■ TiO₂/ZnO/Fe₂O₃, ■ TiO₂/ZnO, ■ TiO₂.



Photocatalytic activity

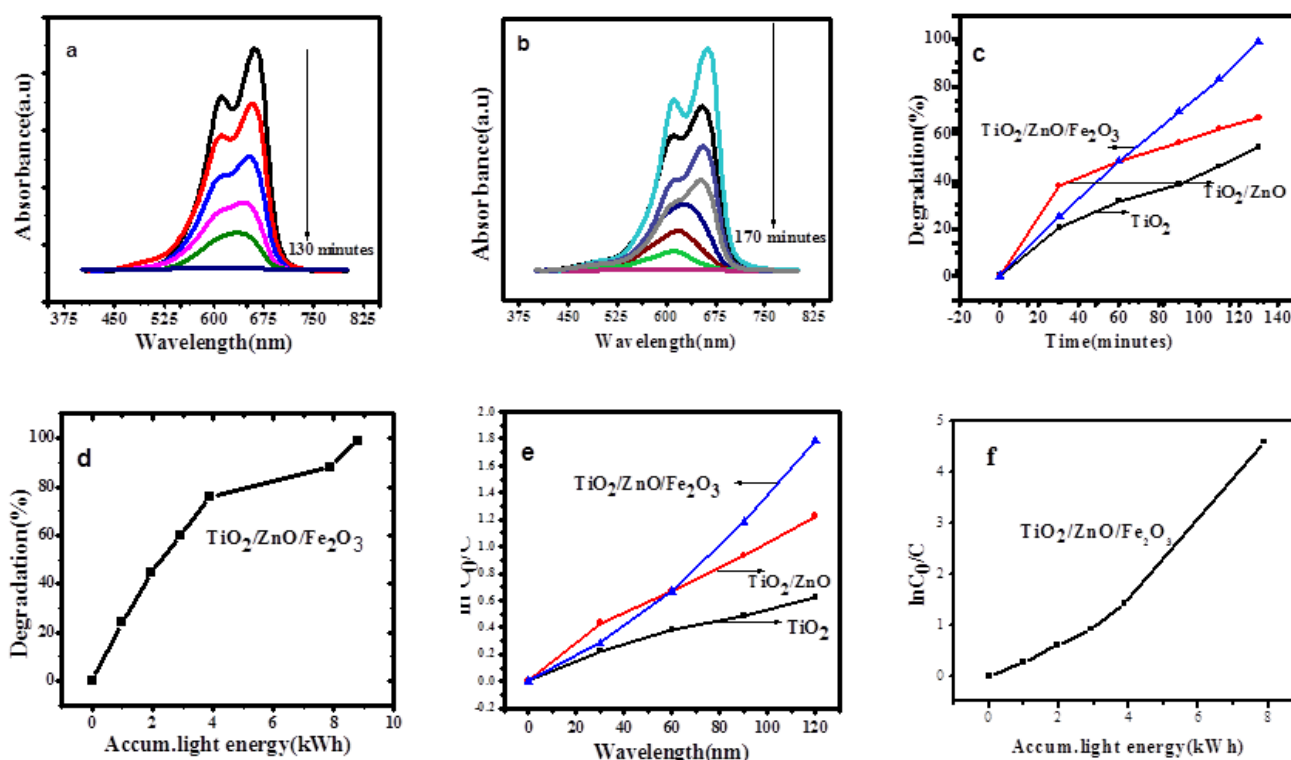
Ultraviolet and sunlight irradiation on a 10 M-4 M methylene blue solution was used to test the photocatalytic dye degradation activity. The complete degradation of methylene blue under UV irradiation using TiO₂/ZnO/Fe₂O₃ catalyst occurred within a period of 130 minutes (Figures 4a-4f). However, on sunlight irradiation using the same catalyst complete mineralization was achieved within 170 minutes, and its corresponding absorption spectra are indicated in Figure 4b. Evaluation of the photocatalytic dye degradation experiment was performed using the equation in C₀/C=k_t. The photocatalysis followed first-order kinetics. The values of the rate constant and regression constant are presented in Table 1. The degradation percentage was calculated using the following equation.

$$\text{Degradation percentage} = ((A_0 - A_t) / A_0) \times 100\%$$

Where A₀ and A_t represents the absorbance of methylene blue at the time 0 and t respectively. The order of photocatalytic activity of the catalyst was as follows, TiO₂<TiO₂/ZnO<TiO₂/ZnO/Fe₂O₃. This affirms the formation of

ternary composites has resulted in a significant enhancement in photocatalytic activities. The improved photocatalytic activity of TiO₂/ZnO/Fe₂O₃ nanocomposite can be mainly attributed to the reduction in the band gap of the ternary nanocomposite. Alongside, as observed from the surface studies, the higher surface area of the ternary composite is a contributing factor to the high photocatalytic efficiency. PL intensity of TiO₂/ZnO/Fe₂O₃ was lowered in comparison to the other two samples indicating the slow rate of electron-hole recombination taking place in the samples in this category [36]. All these facts account to the highest photocatalytic activity of TiO₂/ZnO/Fe₂O₃ nanocomposites.

Figure 4. UV absorption Spectra of photocatalytic degradation of methylene blue in the presence of (a) UV light irradiation (b) Sunlight irradiation (c) Percentage of degradation of methylene blue under UV irradiation and (d) Percentage of degradation of methylene blue under sunlight irradiation (e) $\ln C_0/C$ versus time of methylene blue degradation under UV irradiation (f) $\ln C_0/C$ versus time of Methylene blue degradation under sunlight irradiation. Note: ■ TiO₂/ZnO/Fe₂O₃, ■ TiO₂/ZnO, ■ TiO₂.



Mechanism

The matching band structure of TiO₂, ZnO, and Fe₂O₃ is a favourable condition for the effective charge transfer [37]. The coupling of semiconductors helped in improving the visible light sensitivity and suppressing the electron-hole recombination and promoting the interfacial charge transfer [38]. In order to describe the mechanism of photocatalytic dye degradation prior knowledge of the band edge position of the conduction band and valence band of TiO₂, ZnO and Fe₂O₃ should be acquired. Before formation of ternary system, both the conduction band edge and valence band edge level of Fe₂O₃ were placed in between that of ZnO [39]. As Fe₂O₃ comes in contact with ZnO, there occurs a shift in the energy bands of ZnO and Fe₂O₃ till the Fermi level attains equilibrium [40-42]. So, on irradiation, the electrons continue to transfer from the conduction band of Fe₂O₃ to that of ZnO and TiO₂. The conduction band edge and valence band edge of ZnO are slightly higher than that of TiO₂ [43]. At the same time, the holes from the valence band of TiO₂ are transferred

to the valence band of Fe_2O_3 and ZnO enhancing the effective spatial charge separation. Both the electrons and holes play a vital role in methylene blue degradation. The holes react with water molecules adsorbed on the surface to produce hydroxyl radicals whereas the photogenerated electrons reacting with the adsorbed oxygen produce superoxide anions. The hydroxyl radicals and superoxide anions have the ability to decompose the dyes. Thus, the ternary system acts as an efficient photocatalytic system by inhibiting electron-hole recombination.

CONCLUSION

The study can be summarized as follows, binary and ternary metal oxide nanocomposites have been successfully synthesized incorporating TiO_2 , ZnO , and Fe_2O_3 metal oxides through a facile sol-gel method. The synthesized samples were subjected to various studies in order to depict their photocatalytic performance in methylene blue degradation. X-Ray Diffraction study confirmed the mixed growth of metal oxide powders in the multiphase composite category. The measurements obtained from SAED patterns were in consistent with planes calculated from XRD. Brunauer-Emmett-Teller analysis revealed a predominant increase of surface area in $\text{TiO}_2/\text{ZnO}/\text{Fe}_2\text{O}_3$ composite in comparison to that of TiO_2 and TiO_2/ZnO . It was inferred from the study that $\text{TiO}_2/\text{ZnO}/\text{Fe}_2\text{O}_3$ nanocomposite possesses visible light sensitivity, enhanced charge separation, and high surface area than the other two compound systems. The aforementioned factors shaped $\text{TiO}_2/\text{ZnO}/\text{Fe}_2\text{O}_3$ nanocomposite, a far superior candidate than the bare TiO_2 and TiO_2/ZnO in the photocatalytic performance of methylene blue degradation. The complete mineralization of the dye in the presence of UV light was achieved within a period of 130 minutes is one of the major findings of the study alongside with the degradation of the same concentration of the dye in direct sunlight within a period of 170 minutes.

REFERENCES

1. Pathak C, et al. Impact of environmental pollution on human future. *J of Environ Pollu.* 2011;2:8-10.
2. Ehrampoush MH, et al. Removal of Methylene blue dye from textile synthetic wastewater using $\text{TiO}_2/\text{UV-C}$ photocatalytic process. *AJBAS.* 2010;4:4279-4285.
3. Sangpour P, et al. Photoenhanced degradation of methylene blue on cosputtered $\text{M}:\text{TiO}_2$ ($\text{M}=\text{Au}, \text{Ag}, \text{Cu}$) nanocomposite systems: A comparative study. *J Phys Chem C.* 2010;114:13955-13961.
4. Alkaykh S, et al. Photocatalytic degradation of methylene blue dye in aqueous solution by MnTiO_3 nanoparticles under sunlight irradiation. *Heliyon.* 2020;6:e03663.
5. Abbasi M, et al. Sonochemical degradation of basic blue 41 dye assisted by nano TiO_2 and H_2O_2 . *J Hazard Mater.* 2008;153:942-947.
6. Zaghbani N, et al. Removal of Safranin T from wastewater using micellar enhanced ultrafiltration. *Desalination.* 2008;222:348-356.
7. Sarria V, et al. Degradation of a biorecalcitrant dye precursor present in industrial wastewaters by a new integrated iron (III) photoassisted-biological treatment. *Appl Catal B Environ.* 2003;40:231-246.
8. Ibhaddon AO, et al. Heterogeneous photocatalysis: Recent advances and applications. *Catalysts.* 2013;3:189-218.
9. Haque MM, et al. TiO_2 -mediated photocatalytic degradation of a textile dye derivative, bromothymol blue, in aqueous suspensions. *Dyes and Pigments.* 2007;75:443-448.
10. Jaihindh DP, et al. Reduced graphene oxide-supported Ag-loaded Fe-doped TiO_2 for the degradation mechanism of methylene blue and its electrochemical properties. *RSC Adv.* 2018;8:6488.

11. Wei M, et al. Nanocrystalline TiO₂ composite films for the photodegradation of formaldehyde and oxytetracycline under visible light irradiation. *Molecules*. 2017;22:950.
12. Sridharan K, et al. Novel visible light active graphitic C₃N₄-TiO₂ composite photocatalyst: Synergistic synthesis, growth and photocatalytic treatment of hazardous pollutants. *Appl Catal B: Environ*. 2013;142:718-728.
13. Khan SB, et al. Exploration of CeO₂ nanoparticles as a chemi-sensor and photo-catalyst for environmental applications. *Sci Total Environ*. 2011;85:943-949.
14. Sin JC, et al. Fabrication of erbium-doped spherical-like ZnO hierarchical nanostructures with enhanced visible light-driven photocatalytic activity. *Mater Lett*. 2013;91:1-4.
15. Diaz-Angulo J, et al. Coupling of heterogeneous photocatalysis and photosensitized oxidation for diclofenac degradation: role of the oxidant species. *J Photo and Photobio A: Chem*. 2019;383:112015.
16. Li M, et al. Direct synthesis of monodispersed ZnO nanoparticles in an aqueous solution. *Mater Lett*. 2007;61:690-693.
17. Cimitan S, et al. Solvothermal synthesis and properties control of doped ZnO nanoparticles. *J of Coll and Int Sci*. 2009;329:73-80.
18. Huang JL, et al. Applications of ZnO in organic and hybrid solar cells. *Energy Environ Sci*. 2011;10:3861-3877.
19. Darzi SJ, et al. Investigation of phase transformations and photocatalytic properties of sol-gel prepared nanostructured ZnO/TiO₂ composites. *J Alloys Compd*. 2009;486:805-808.
20. Marcı G, et al. Preparation characterization and photocatalytic activity of polycrystalline ZnO/TiO₂ systems. 2. surface, bulk characterization, and 4-Nitrophenol photodegradation in liquid–solid regime. *J Phys Chem B*. 2001;105:1033-1040.
21. Chen XQ, et al. Preparation and photocatalytic properties of Fe-doped TiO₂ nanoparticles. *J Cent South Univ Technol*. 2004;11:161-165.
22. Volfova L. Tailoring photocatalytic activity of TiO₂ nanosheets by ⁵⁷Fe. *J Phys Chem C*. 2020;12:6669-6682.
23. Mei Q, et al. TiO₂/Fe₂O₃ heterostructures with enhanced photocatalytic reduction of Cr (VI) under visible light irradiation. *RSC Adv*. 2019;9:22764-22771.
24. Parashar M, et al. Metal oxides nanoparticles *via* sol-gel method: a review on synthesis, characterization and applications. *J Mater Sci: Mater Electron*. 2020;31:3729-3749.
25. Tian J, et al. Preparation and characterization of TiO₂, ZnO, and TiO₂/ZnO nanofilms *via* sol-gel process. *Cera Inter*. 2009;35:2261-2270.
26. Jing He, et al. Facile formation of anatase/rutile TiO₂ nanocomposites with enhanced photocatalytic activity. *Molecules*. 2019;24:2996.
27. Lin L, et al. A highly efficient TiO₂@ZnO n-p-n heterojunction nanorod photocatalyst. *Nanoscale*. 2013;5:588-593.
28. Sharma B, et al. TiO₂-Fe₂O₃ nanocomposite heterojunction for superior charge separation and the photocatalytic inactivation of pathogenic bacteria in water under direct sunlight irradiation. *J Environ Chem Engin*. 2018;6:134-145.
29. Bouhjar F, et al. Hydrothermal fabrication and characterization of ZnO/Fe₂O₃ heterojunction devices for hydrogen production. *J Anal Pharm Res*. 2018;7:315-321.
30. Li X, et al. Extraction of iron from vanadium slag using pressure acid leaching. *Proced Environ Scien*. 2016;31:582-588.

31. Mazinani B, et al. Photocatalytic activity, surface area and phase modification of mesoporous SiO₂-TiO₂ prepared by a one-step hydrothermal procedure. *Cera Inter*. 2014;40:11525-11532.
32. Xia Y, et al. Core-shell structured α -Fe₂O₃@TiO₂ nanocomposites with improved photocatalytic activity in the visible light region. *Phys Chem Chem Phys*. 2013;15:18627-18634.
33. Wen L, et al. Synthesis, characterization, and photocatalysis of Fe-doped: A combined experimental and theoretical study. *Inter J of Photo*. 2012:2012.
34. Jaihindh DP, et al. Reduced graphene oxide-supported Ag-loaded Fe-doped TiO₂ for the degradation mechanism of methylene blue and its electrochemical properties. *RSC Adv*. 2018; 8:6488-6501.
35. Yu JC, et al. Photocatalytic activity, antibacterial effect, and photoinduced hydrophilicity of TiO₂ films coated on a stainless steel substrate. *Environ Sci Technol*. 2003;7:22-96.
36. Shwetharani R, et al. Recent advances and strategies to tailor the energy levels, active sites and electron mobility in titania and its doped/composite analogues for hydrogen evolution in sunlight. *Catal Sci Technol*. 2019;9:12-46.
37. Munawar K, et al. Single step fabrication of CuO-MnO-2TiO₂ composite thin films with improved photoelectrochemical response. *RSC Adv*. 2017;7:15885-15893.
38. Gao J, et al. Preparation of Er³⁺:YAlO₃/Fe-doped TiO₂-ZnO and its application in photocatalytic degradation of dyes under solar light irradiation. *Desalination*. 2011;268:68-75.
39. Tama AM, et al. MoS₂ nanosheet incorporated α -Fe₂O₃/ZnO nanocomposite with enhanced photocatalytic dye degradation and hydrogen production ability. *RSC Adv*. 2019;9:40357-40367.
40. Kaneti YV, et al. Solvothermal synthesis of ZnO-decorated α -Fe₂O₃ nanorods with highly enhanced gas-sensing performance toward n-butanol. *J Mater Chem A*. 2014;2:13283-13292.
41. Tama AM, et al. MoS₂ nanosheet incorporated α -Fe₂O₃/ZnO nanocomposite with enhanced photocatalytic dye degradation and hydrogen production ability. *RSC Adv*. 2019;9:40357-40367.
42. Liu X, et al. Investigation of photocatalytic activities over ZnO-TiO₂-reduced graphene oxide composites synthesized via microwave-assisted reaction. *J Coll and Inter Scie*. 2013;394:441-444.
43. Darzi SJ, et al. Investigation of phase transformations and photocatalytic properties of sol-gel prepared nanostructured ZnO/TiO₂ composites. *J of Alloys Comp*. 2009;486:805-808.